JOURNAL OF GEOPHYSICAL RESEARCH, VOL. 113, A12203, doi:10.1029/2008JA013248, 2008

Ion composition in the plasma trough and plasma plume derived from a Combined Release and Radiation Effects Satellite magnetoseismic study

Kazue Takahashi,[1] Shin-ichi Ohtani,[1] Richard E. Denton,[2] W. Jeffrey Hughes,[3] and Roger R. Anderson[4]

Received 3 April 2008; revised 22 July 2008; accepted 15 September 2008; published 5 December 2008.

[1] The mass and energy carried in the magnetosphere by heavy ions, O^+ in particular, are known to increase as geomagnetic activity increases. However, the ion composition in the magnetosphere has not been fully specified since measurements of the flux of different ion species from the ionospheric thermal energy (below 1 eV) to the ring current energy (above 100 keV) are difficult with single-particle instruments. We used mass density determined by a magnetoseismology technique and the electron density derived from measured plasma wave spectra to investigate the ion composition and total mass density for Combined Release and Radiation Effects Satellite (CRRES) orbit 962 (27–28 August 1991). This orbit occurred during a geomagnetic storm and included afternoon passes through the plasmasphere, the plasma trough, and a plasma plume, where these plasma regions were identified using the electron density n_e. In the magnetoseismology analysis, we determined the fundamental frequency of the toroidal standing Alfvén waves f_{T1} from the electric and magnetic field data and then inferred the corresponding total mass density ρ_{total} at the satellite by solving an MHD wave equation with a realistic magnetic field model and a realistic assumption for the mass distribution along the field line. The value of f_{T1} changed little when the spacecraft moved between the plasma trough and the plasma plume, implying the dominance of heavy ions in the plasma trough. From the values of n_e and ρ_{total}, we derived quantities associated with O^+ by assuming that the plasma consisted of three ions, H^+, He^+, and O^+. In the plasma trough, O^+ ions are found to carry a number density of $\sim$10 cm^{-3}, $\sim$50% of the number density, and $\sim$90% of the mass density. On the other hand, O^+ is found to be much less dominant in the plasma plume. Our results are consistent with DE-1 studies of the formation of an oxygen torus at the outer edge of the H^+ plasmapause during geomagnetic active periods and with GEOS-1 and GEOS-2 studies that reported strong dependence of O^+ density on geomagnetic activity and on solar extreme ultraviolet flux. In addition, our events indicate that the plasma plume boundary, defined in terms of the number density of electrons or light ions (H^+ and He^+), may not exhibit similar structure in the total mass density that can be readily detected using magnetoseismology techniques.

Citation: Takahashi, K., S. Ohtani, R. E. Denton, W. J. Hughes, and R. R. Anderson (2008), Ion composition in the plasma trough and plasma plume derived from a Combined Release and Radiation Effects Satellite magnetoseismic study, *J. Geophys. Res.*, *113*, A12203, doi:10.1029/2008JA013248.

1. Introduction

[2] The magnetospheric plasma consists of multiple ion species. Observing the spatial and temporal variations of the density of each ion species is important in understanding the source region of the ions and the role the ions play in controlling the properties of the ring current and the radiation belt. Of particular importance are O^+ ions, which originate from the ionosphere and affect both MHD and kinetic processes in the equatorial magnetosphere. A few of the major reasons for studying O^+ ions are as follows.

[3] 1. Energetic electrons (energy > 100 keV) follow drift paths that are determined primarily by the ambient magnetic

[1]Applied Physics Laboratory, Johns Hopkins University, Laurel, Maryland, USA.
[2]Department of Physics and Astronomy, Dartmouth College, Hanover, New Hampshire, USA.
[3]Department of Astronomy, Boston University, Boston, Massachusetts, USA.
[4]Department of Physics and Astronomy, University of Iowa, Iowa City, Iowa, USA.

0148-0227/08/2008JA013248$09.00

field, **B**. Strong deformation of **B** by the ring current leads to enhanced loss of radiation belt particles to the magnetosheath [*Ukhorskiy et al.*, 2006]. Heavy ions (O^+ in particular) are known to become a major carrier of the storm time ring current [*Daglis et al.*, 1999]. The answer to the question of how ionospheric O^+ ions gain ring current energy (1−100 keV) and are transported to the ring current region is important for understanding electron loss.

[4] 2. MHD-wave-mediated transport of electrons depends on the mass density and ion composition. For given electron number density, higher concentration of heavy ions (He^+ and O^+) means higher mass density. Drift resonance ($\omega - m\omega_d = 0$, for an axisymmetric magnetosphere) of radiation belt electrons with low-m ultra-low frequency (ULF) waves in the 1- to 10-mHz band leads to acceleration and radial transport of the electrons, where m is the azimuthal wave number [*Elkington et al.*, 1999]. For standing Alfvén waves the frequency ω depends on the ion mass density (thus on the ion composition). Consequently, the energy of resonant electrons depends on the ion mass (and composition).

[5] 3. The growth of electromagnetic ion cyclotron (EMIC) waves depends on the ion composition [*Kozyra et al.*, 1984; *Jordanova et al.*, 2007]. EMIC waves are observed in the inner magnetosphere during geomagnetic storms [*Bräysy et al.*, 1998; *Erlandson and Ukhorskiy*, 2001] and the waves can scatter the pitch angle of radiation belt electrons, leading to loss of the electrons into the neutral atmosphere. The lack of reliable ion composition models is a major problem in evaluating the EMIC mechanism for the electron loss [*Meredith et al.*, 2003]. It is obvious that improved measurements of O^+ ion density will lead to a better understanding of the above magnetospheric processes.

[6] Previous particle observations near the magnetic equator studied ion composition and its dependence on solar radiation and geomagnetic activity [*Young et al.*, 1982; *Roberts et al.*, 1987; *Nosé et al.*, 2001]. However, the particle instruments used in these studies had limited energy and pitch angle windows and a limited capability to distinguish ion species. On the other hand, we can indirectly probe the plasma mass density from the spectral properties of ULF waves. The idea of using ULF wave signals to estimate magnetospheric mass distribution is at least half a century old [*Obayashi and Jacobs*, 1958].

[7] The principle for this technique, termed normal mode magnetoseismology [*Chi and Russell*, 2005], is simple. Alfvén waves propagate along the ambient magnetic field and their velocity is given by

$$V_A = B(\mu_0 \rho_{\text{total}})^{-1/2} \tag{1}$$

where B is the magnetic field intensity, μ_0 is the permeability of free space, and ρ_{total} is the total mass density of the plasma. This means that the frequency of standing Alfvén waves depends on the magnetic field intensity, field line length, and mass density variation along the magnetic field. Conversely, if we know the magnetic field and the functional form of mass density variation along the field line, we can relate the observed frequency to the mass density. It usually requires a numerical technique to solve the wave equation for the frequency-density relation in realistic geomagnetic field and plasma distribution geometry [e.g., *Singer et al.*, 1981].

[8] Normal mode magnetoseismology has proven to be a particularly powerful tool in investigating the global density structure. In the last decade there has been considerable progress in this technique owing much to the use of the gradient method [*Baransky et al.*, 1985] and the cross-phase technique [*Waters et al.*, 1991] to detect standing wave frequencies on the ground and also owing to the improved models of the background magnetic field and mass distribution along the magnetic field line [*Denton and Gallagher*, 2000; *Takahashi et al.*, 2004; *Takahashi and Denton*, 2007].

[9] When an independent measurement of electron number density is available, we can combine it with the mass density derived with magnetoseismology to gain valuable information on heavy ion distribution in the magnetosphere. The electron number density is commonly estimated using two features of plasma waves that are observed in situ by spacecraft [*LeDocq et al.*, 1994]. One is the cutoff of continuum radiation that occurs at the plasma frequency f_{pe}, which is given by

$$f_{pe} = (2\pi)^{-1}\left(n_e e^2/\varepsilon_0 m_e\right)^{1/2} \tag{2}$$

where e is the electron charge, m_e is the electron mass, and ε_0 is the permittivity of free space. The other is the narrowband emission at the upper hybrid resonance frequency f_{UHR}, which is given by

$$f_{\text{UHR}} = \left(f_{pe}^2 + f_{ce}^2\right)^{1/2} = (2\pi)^{-1}\left\{\left(n_e e^2/\varepsilon_0 m_e\right) + (eB/m_e)^2\right\}^{1/2} \tag{3}$$

where f_{ce} is the electron cyclotron frequency. The value of B that is necessary to determine f_{ce} is usually measured with a magnetic field experiment.

[10] Using the mass density ρ_{total} and the electron number density n_e we can determine the average ion mass M that is defined as

$$\rho_{\text{total}} = n_e m_e + \Sigma n_i m_i \sim \Sigma n_i m_i \equiv n_e M \tag{4}$$

where n_i and m_i are the number density and mass of the ith ion species, respectively. The value of M is 1.0 amu for a pure H^+ plasma and 16.0 amu for a pure O^+ plasma. In reality, M is somewhere between these two limits and M is a convenient measure of the overall contribution of heavy ions to the magnetospheric plasma. Furthermore, in cases where we know the density ratios among the major ion species (H^+, He^+, O^+), it is possible to use the ratios as a constraint to determine the density for individual ions.

[11] Studies that compared mass density determined with magnetoseismology and electron number density determined from plasma wave spectra confirmed that the heavy ion density in the inner magnetosphere increases during geomagnetic storms [e.g., *Takahashi et al.*, 2006; *Dent et al.*, 2006]. With the heavy ions playing a role in physical processes during the development of storms and substorms, magnetoseismology makes a vital contribution to our understanding of these dynamic phenomena.

[12] Although magnetoseismology detects the latitudinal variation of mass density across the plasmapause [*Milling et al.*, 2001; *Menk et al.*, 2004; *Dent et al.*, 2006; *Kale et al.*, 2007], it is not clear if the technique is useful in detecting

the plasma (drainage) plume boundary. Global images from the IMAGE spacecraft [*Sandel et al.*, 2001] have changed our notion of the plasmasphere from a quasi-steady structure to a highly dynamic region with interesting features such as fingers and drainage plumes, although some of these structures have been predicted [*Grebowsky*, 1970] and observed in situ as detached plasma [*Chappell*, 1974]. By following the location of the plume we can learn a great deal about the magnetospheric electric field [*Spasojevic et al.*, 2003].

[13] One goal of the present study is to determine if there is a strong change in mass density across plasma plume boundaries that leads to a rapid change of standing Alfvén wave frequencies. If the frequency change does occur, it will be a strong demonstration that ground-based magnetoseismology is useful for studying the plume dynamics. This is an important question since heavy ions (O^+, in particular) may cause the total mass density radial gradient to be quite different from that of the electron (or H^+) density gradient as was reported for a plasmapause crossing by the DE-1 satellite [*Fraser et al.*, 2005]. Recently, *Abe et al.* [2006] interpreted ULF pulsation signals detected by two latitudinally separated stations in terms of plasma plume density structure. We use spacecraft observations to test if magnetoseismology is useful in detecting plumes.

[14] In this paper we present a magnetoseismology study of the mass density of a plasma drainage plume that was encountered by the Combined Release and Radiation Effects Satellite (CRRES) spacecraft. Contrary to our expectation, we found that the mass density changed little across the plume boundary that is defined in terms of the electron number density. This happened because outside the plasma plume a high concentration of heavy ions compensated for the lower plasma number density. We conclude that the boundary could not have been detected using ground-based magnetoseismology. We also discuss the implication of the analysis results to heavy ion transport in the inner magnetosphere.

[15] The remainder of this paper is organized as follows. Section 2 describes the data. The discussion is presented in section 3, and the conclusions are presented in section 4.

2. Data

[16] CRRES operated for 15 months in 1990–1991 on a $1.05 \times 6.3\ R_E$ elliptical orbit with an inclination of 18°, an orbital period of 10 hr, and a spin period of 30 s. The data presented in this paper were acquired on CRRES orbit 962, which spanned a time period from ~2100 UT of 27 August (day of year 239) to ~0700 UT of 28 August 1991. The experiments used for the data are the fluxgate magnetometer instrument [*Singer et al.*, 1992], the electric field/Langmuir probe instrument (referred to as the electric field experiment) [*Wygant et al.*, 1992], and the plasma wave experiment [*Anderson et al.*, 1992].

[17] The electric and magnetic field data used in the ULF wave analysis are spin (~30-s) averages sampled twice per spin, resulting in an ~15-s time resolution. The electric field measurements were made in the spin plane of the spacecraft. The third component, directed along the satellite's spin axis (maintained at a small angle with respect to the Earth-Sun line), was derived using the assumption $\mathbf{E} \cdot \mathbf{B} = 0$. This technique is reliable when the magnetic field vector makes an angle greater than 20 degrees from the spin plane, which was satisfied on most of CRRES orbit 962. For the purpose of finding standing Alfvén waves with different polarizations, we have rotated the **E** and **B** fields into a local coordinate system in which $\mathbf{e}_z$ is along the 150-s running average of the measured magnetic field vector, $\mathbf{e}_y$ (eastward) is the perpendicular to $\mathbf{e}_z \times \mathbf{R}$, where **R** is the geocentric radial vector to the spacecraft position, and $\mathbf{e}_x$ (outward) completes a right-handed orthogonal system *x*-*y*-*z*. The removal of the running average is equivalent to convolution of the input time series with the time-domain weight function $\delta(t) - u(t)$, where $\delta(t)$ is the delta-function and $u(t)$ is a boxcar function. In the frequency domain this process modifies the input signal by a factor that is the Fourier transform of the weight function, $1 - \sin(\pi fT)/(\pi fT)$, where f is frequency and T is the length (=150 s) of the boxcar function. The filter does not alter the phase of the input signal but reduces its amplitude by more than 50% below ~5 mHz.

[18] The plasma wave data used in this study were acquired with the sweep frequency receiver (SFR) of the plasma wave experiment. The receiver processed the electric field signals that were detected with a 100-m tip-to-tip wire antenna deployed in the spin plane of the spacecraft in a frequency range of 100 Hz to 400 kHz divided into four bands (SFR-1 through SFR-4, each consisting of 32 frequency steps). Frequency sweeping was done every 32 s in SFR-1, 16 s in SFR-2, and 8 s in SFR-3 and SFR-4.

2.1. Solar and Geomagnetic and Conditions

[19] Known factors that control the plasma mass density and the ion composition include the solar radiation and geomagnetic storm intensity. In order to put our observations in the context of these factors we show in Figure 1 the daily solar extreme ultraviolet flux index $F_{10.7}$ provided by NOAA (ftp://ftp.ngdc.noaa.gov/STP/SOLAR_DATA), hourly solar wind parameters provided as the OMNI2 data set by NASA/NSSDC (http://omniweb.gsfc.nasa.gov/), and the hourly *Dst* index provided by the World Data Center at Kyoto University (http://swdcwww.kugi.kyoto-u.ac.jp/) for a 10-day period that includes CRRES orbit 962. Year 1991 was near a solar activity maximum, which is reflected in the elevated value ~200 (in the unit of 10^{-22}W m^{-2} Hz^{-1}) of $F_{10.7}$. In contrast, $F_{10.7}$ is below 100 around a solar minimum.

[20] The orbit (highlighted by shading) occurred during a small geomagnetic storm that started with a positive *Dst* impulse at ~1500 UT on day 239 (27 August 1991). The value of *Dst* reached a minimum of about −60 nT at ~2300 UT on day 239, nearly coincident with the beginning of CRRES orbit 962. This geomagnetic storm was associated with the arrival of a solar wind structure characterized by a velocity increase from 330 km/s to 460 km/s, a peak density of 31 cm^{-3}, a peak dynamic pressure of 13 nPa, and a peak magnetic field magnitude of 28 nT. The structure accompanied a southward magnetic field. We believe that these solar wind and interplanetary magnetic field (IMF) conditions led to enhancement of plasma convection in the magnetosphere and formation of a plasma plume in the manner previously described by model calculations and satellite observations [*Grebowsky*, 1970; *Elphic et al.*, 1996; *Spasojevic et al.*, 2003; *Moldwin et al.*, 2004; *Goldstein and Sandel*, 2005].

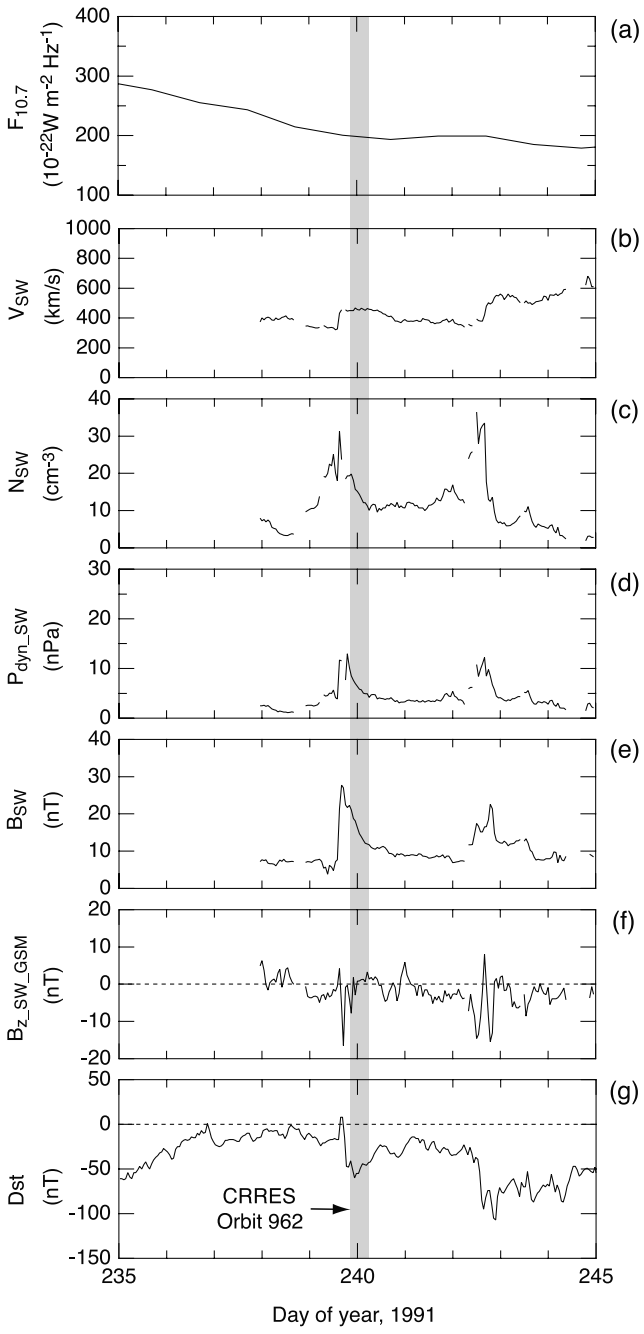

Figure 1. Solar wind and geomagnetic condition for a 10-day interval in 1991 that includes CRRES orbit 962 (highlighted by shading). (a) Solar 10.7-cm radio flux $F_{10.7}$. (b) Solar wind bulk velocity. (c) Solar wind number density. (d) Solar wind dynamic pressure. (e) Solar wind magnetic field magnitude. (f) GSM southward component of the solar wind magnetic field. (g) The *Dst* index. The time resolution is 1 day for $F_{10.7}$ and 1 hour for the other parameters.

2.2. Spectra of ULF Waves and Plasma Waves

[21] Figure 2 shows the spectral properties of ULF waves (0−20 mHz) and plasma waves (10−400 kHz) on CRRES orbit 962. This figure covers a 9-hr segment of the 10-hr orbital period and is approximately centered on apogee. The spacecraft location is shown at the bottom, where the *L* shell parameter, magnetic latitude (MLAT), and magnetic local time (MLT), were calculated assuming a centered dipole.

[22] Figure 2a shows the electric field power spectral density measured by the SFR of the plasma wave experiment. We show only the frequency range 10−400 kHz, corresponding to the two bands SFR-3 (6.4−50 kHz) and SFR-4 (50−400 kHz). Notable features in the spectra include narrowband emissions at the upper hybrid resonance frequency (labeled f_{UHR}) and cutoff at the plasma frequency (labeled f_{pe}) of continuum radiation.

[23] Sudden changes in f_{pe} or f_{UHR} occurred twice each on the inbound and outbound legs of the spacecraft orbit. We attribute these changes to crossings of the plasmapause (21:50 UT and 05:50 UT) and the boundary between the plasma trough and the plasma plume (23:20 UT and 04:40 UT). As Figure 1 showed, a magnetic storm was in progress following the arrival of the solar wind plasma with high dynamic pressure and southward magnetic field. It is thus reasonable to assume that the magnetospheric electric field increased before the start of orbit 962 and produced a plasma plume.

[24] Figures 2b−2e show the spectral properties of the outward component of the electric field E_x and the eastward component of the magnetic field B_y. The power spectra were computed using a Fourier transform method [*Bendat and Piersol*, 1971] with a moving time window 25 min long and a degree of freedom of 6. Note that by definition, the magnetic field data are a high-pass filtered version of the original data, that is, the original minus 150-s running averages. By contrast, the electric field data were not filtered except that we removed the best-fit second-order polynomial from each 25-min segment.

[25] The E_x spectra (Figure 2b) show a narrowband oscillation below 10 mHz, labeled f_{T1}, from 2200 UT on day 239 to 0520 UT on day 240. The frequency of this oscillation changed smoothly along the orbit, starting from ~7 mHz at 2200 UT, reaching a minimum of ~2 mHz as the spacecraft reached its apogee (~0200 UT), and then moving up to ~6 mHz (0520 UT) as the spacecraft moved back closer to the Earth. The spectral line is attributed to the fundamental toroidal standing Alfvén waves (thus the label f_{T1}), which is commonly observed in the magnetosphere [*Junginger et al.*, 1984]. The toroidal waves are a natural MHD eigenmode of the inner magnetosphere, characterized by azimuthal field line displacement and a radial electric field [*Radoski and Carovillano*, 1966]. The toroidal oscillations are excited at multiple harmonics, but in the electric field the fundamental mode is usually the strongest near the equator as a result of its equatorial antinode [*Cummings et al.*, 1969]. The power spectra of the B_y component show evidence of the same oscillation around 2300 UT, but the spectral line in this component is not continuously observed unlike in the E_x spectra. The B_y oscillation at the f_{T1} frequency is particularly weak after 0100 UT, when the spacecraft was nearing the magnetic equator, because the wave magnetic field has a node at the magnetic equator.

[26] The relationship between E_x and B_y also supports the toroidal wave interpretation of the narrowband oscillation. Despite the weak appearance of the f_{T1} trace in the B_y spectra, Figure 2d shows high coherence between E_x and B_y at the f_{T1} frequency. Figure 2e shows that, when E_x-B_y coherence is higher than 0.6, the E_x-B_y cross-phase in the f_{T1}

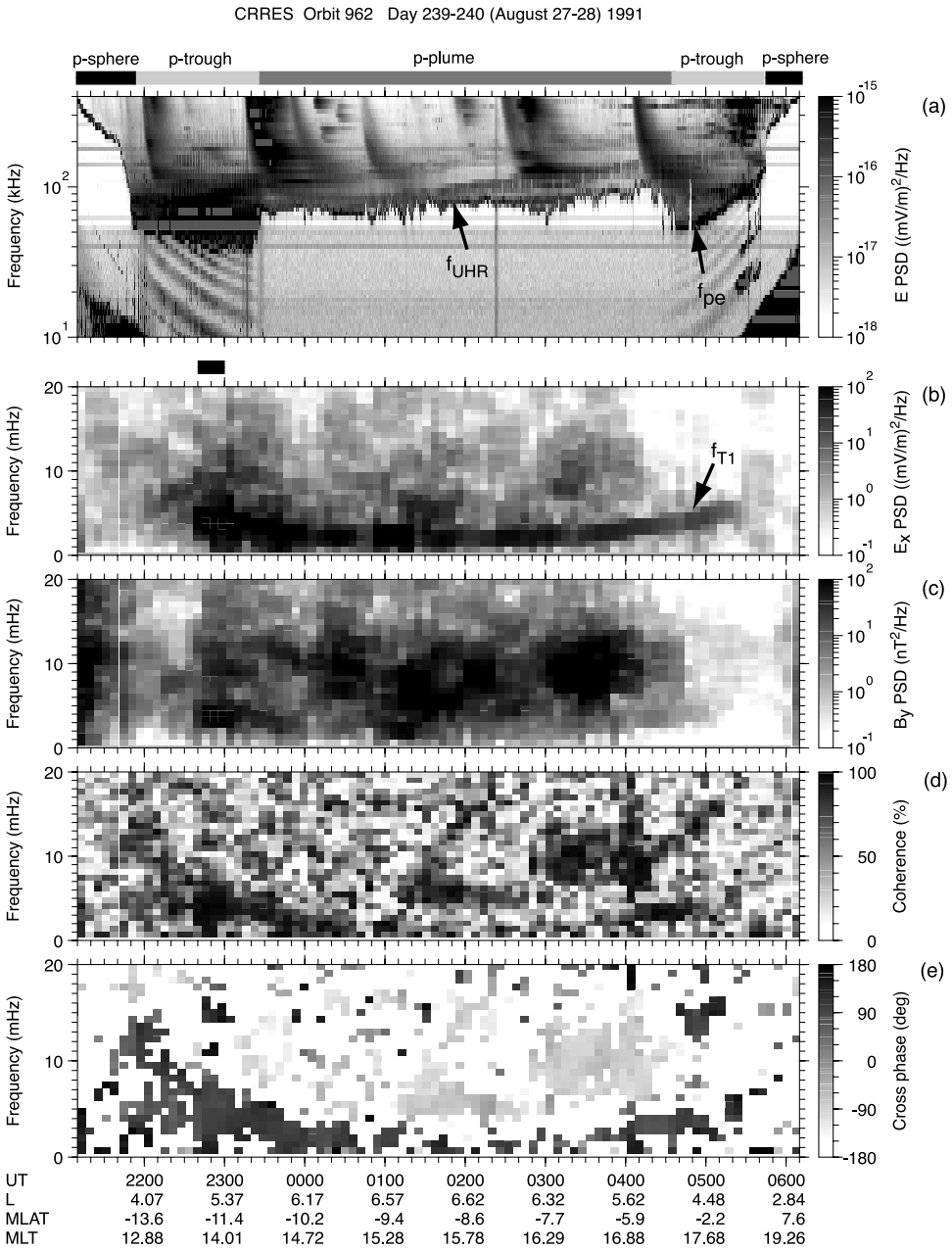

Figure 2. Plasma wave and ULF wave properties for CRRES orbit 962. (a) Electric field power spectral density measured by the sweep frequency receiver (SFR) of the plasma wave experiment. (b–e) Dynamic display of the power spectral density, coherence, and cross-phase of the toroidal components, E_x and B_y, of the electric and magnetic field in the 0- to 20-mHz band generated using data from the electric field and magnetic field experiments. The horizontal bars above Figure 2a indicate the three regions identified according to the electron number density. The short horizontal bar above Figure 2b indicates the 20-min segment shown in Figure 3.

band stays near −90°, consistent with the fundamental mode observed below the magnetic equator.

[27] The major feature to note in Figure 2 is the lack of a sudden change in f_{T1} as the spacecraft moved into and out of the low-density region (plasma trough), that is, the two intervals 2150–2320 UT and 0440–0550 where the f_{pe} trace in Figure 2a indicates a substantially lower electron number density than in the neighboring regions (plasmasphere and plasma trough). This will be examined below in great detail in relation to the ion composition.

[28] Figure 3 shows the time series and spectra for all the field components (except E_z, which is assumed to be zero) for a 20-min interval during toroidal wave activity. Although oscillation is present in all field components (Figure 3a), the spectra (Figure 3b) reveal that the oscillation power is strongest near 3 mHz (labeled f_{T1}). At this frequency the E_x power is clearly higher than the E_y power, implying that the plasma motion (=$\mathbf{E} \times \mathbf{B}$) was primarily azimuthal as is expected for the toroidal mode.

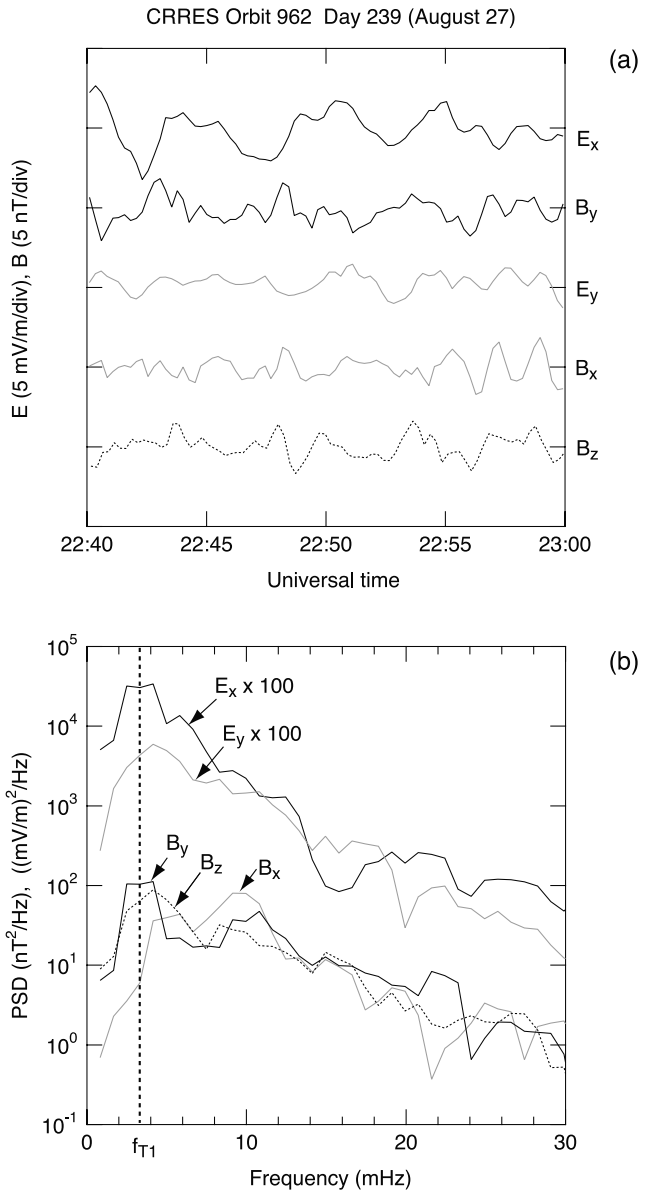

Figure 3. (a) Magnetic and electric fields for a 20-min data segment taken from the outbound leg of CRRES orbit 962. The traces are ordered by polarization: the top pair, E_x and B_y, represents the toroidal components; the second pair, E_y and B_x, the poloidal components; and the bottom trace, the compressional component B_z. (b) The power spectral density (PSD) computed from the time series data shown in Figure 3a. A strong peak occurs in the toroidal components at ~3 mHz as a result of a fundamental toroidal standing Alfvén wave, as indicated by a vertical dashed line labeled f_{T1}.

2.3. Electron Density Global Structure

[29] In referring to the high-n_e region near the CRRES apogee on orbit 962 (Figure 2a) we used the term "plasma plume". We believe that this region identification is justified in light of the geomagnetic activity prior to and during the CRRES observation and in light of published images of magnetospheric density structures taken from the IMAGE spacecraft [e.g., *Goldstein and Sandel*, 2005]. Figures 4a and 4b illustrate geomagnetic activity indices *Kp* and *Dst* for a 2-day period that includes CRRES orbits 960 through 962. Figures 4c and 4d show the L dependence of the electron number density for the three orbits, plotted separately for the outbound and inbound legs. The density data are 1-min averages of the high time resolution (up to 8-s) data that were produced using the technique described by *LeDocq et al.* [1994]. Geomagnetic activity was low during orbit 960, and the electron density for this orbit lacked a clear plasmapause signature, similar to a "saturated plasmasphere" reported by *Carpenter and Anderson* [1992]. Geomagnetic activity started to increase during orbit 961, and this is reflected in the density profile that exhibits a plasmapause at $L \sim 4.5$ (outbound leg) and $L \sim 4$ (inbound leg). In addition, a plasma plume started to form (or drifted to the satellite position) on the inbound leg of orbit 961. The plasmasphere erosion continued during orbit 962, and the plasmapause distance reduced to $L \sim 3.6$ (outbound leg) and $L \sim 3.3$ (inbound leg). By this time the signature of the plasma plume became more obvious, with its inner edge clearly seen at $L \sim 5.8$ (outbound leg) and $L \sim 5.1$ (inbound leg).

[30] The above sequence of n_e observations leads us to a schematic representation of electron density structure shown in Figure 5 for orbit 962. In this figure the orbit segments are marked differently according to the measured electron number density. A plasmasphere with an extended plasma plume is superposed onto the orbit trace in such a way that the location of the region boundary matches the observation. However, since the whole plasma structure changes shape and rotates around the Earth [e.g., *Elphic et al.*, 1996], the illustrated structure does not represent an accurate snapshot of the plasma structure.

2.4. Mass Density and Ion Composition

[31] We derived parameters related to the ion composition by combining the mass density derived using the magnetoseismology technique [*Takahashi et al.*, 2002, 2004; *Takahashi and Denton*, 2007; *Denton and Gallagher*, 2000; *Denton et al.*, 2001, 2004] and electron number density derived from the plasma wave spectra. Four quantities that resulted from CRRES orbit 962 are plotted in Figure 6 as a function of the dipole L value along the satellite orbit (the L value differs somewhat from the equatorial distance of the more realistic model magnetic field lines that were used in solving the wave toroidal wave equation). Separate plots are prepared for the outbound and inbound legs of the orbit considering the local time difference between the legs. The vertical dashed lines mark the center of rapid changes in n_e (light dots in Figures 6c and 6d), which separate the orbit into three segments labeled p-sphere (plasmasphere), p-trough (plasma trough), and p-plume (plasma plume).

[32] Figures 6a and 6b show the fundamental toroidal frequency f_{T1}. This frequency was determined by examining the power spectra of E_x computed using the maximum entropy method (MEM) [*Press et al.*, 1986] with a moving time window 8 min long. The window was stepped forward in 1-min increments. In the MEM technique we fixed the order of the autoregressive process at 6. Broad spectral peaks were rejected by imposing the condition $\Delta f < 3$ mHz, where Δf is the full width of the peak at half maximum. We

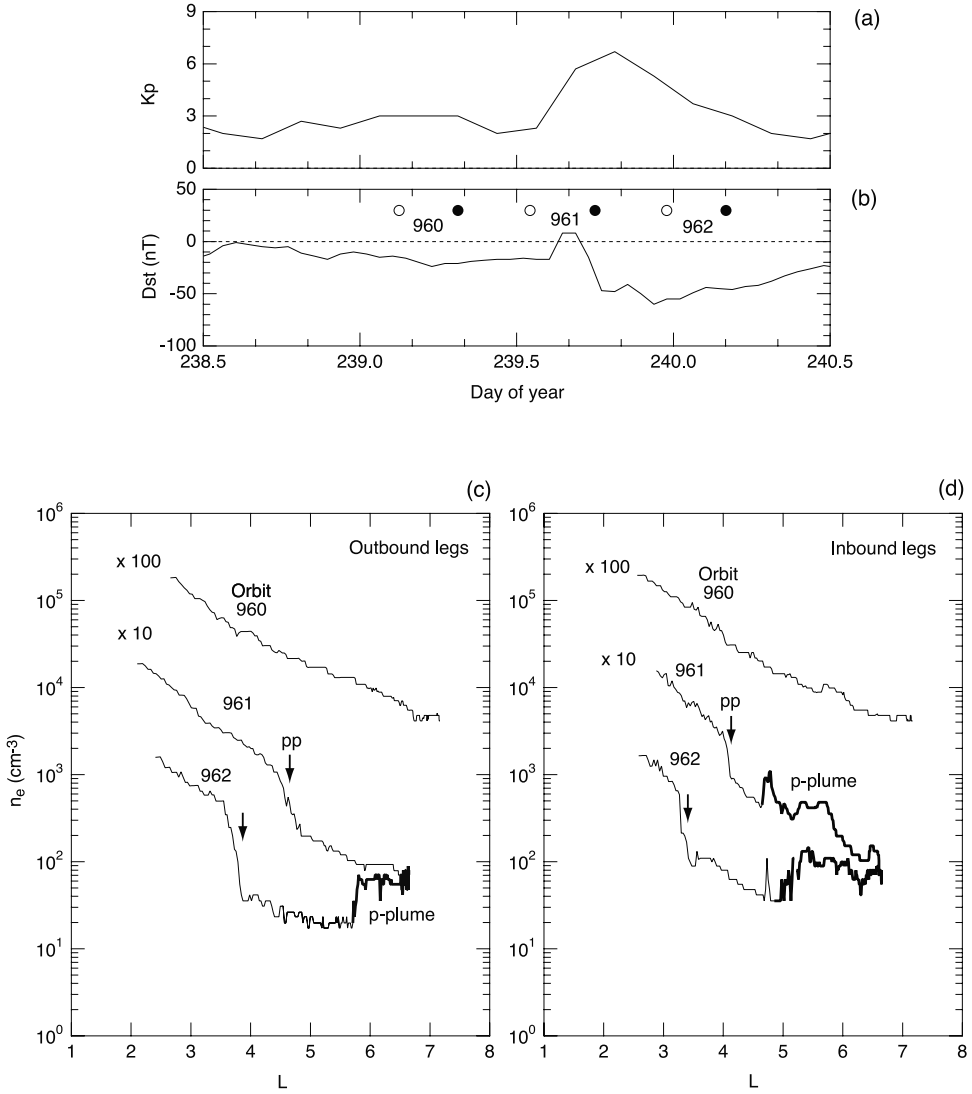

Figure 4. (a) *Kp* index. (b) *Dst* index. The dots indicate the time centers of the outbound (open circle) and inbound (solid circle) legs of CRRES orbits 960 through 962. (c and d) Electron number density plotted as a function of dipole L for inbound and outbound legs of three consecutive CRRES orbits. The electron number density is multiplied by a factor of 10 between orbits to offset the traces. The arrows indicate the plasmapause, and the thick traces indicate the plasma plume. On the outbound portion of the orbit, the plasmapause moved from $L = 4.5$ to $L = 3.7$ and from orbit 961 to 962, and a plasma plume was observed beyond $L = 5.9$ on orbit 962. On the inbound portion of the orbit, a plume is already seen on orbit 961.

also rejected low-amplitude events by imposing the condition $a_{\rm rms} > 0.005$ mV/m for the selected events, where $a_{\rm rms}$ is the root-mean-square amplitude contained in the bandwidth Δf centered on a spectral peak. The final selection of $f_{\rm T1}$ samples was done by generating frequency versus L plots of all spectral peaks that survived the above two conditions and then making final visual rejection of data points that were located away from the $f_{\rm T1}$ trace seen in Figure 2b.

[33] The L dependence of $f_{\rm T1}$ is quite similar between the two orbital legs, and the general trend of decreasing frequency with increasing L is consistent with the well-known statistical L dependence of standing Alfvén wave frequencies. On the outbound leg $f_{\rm T1}$ was detected from $L = 4.2$ to the spacecraft apogee of $L = 6.7$. On the inbound leg $f_{\rm T1}$ was detected from $L = 4.0$ to $L = 6.7$. On both legs $f_{\rm T1}$ decreased monotonically with increasing L, from 8 mHz at $L \sim 4.2$ to 2 mHz at $L \sim 6.7$. Given these $f_{\rm T1}$ profiles, one would conclude that there were no radial stepwise plasma structures in the magnetospheric plasma. This conclusion, of course, depends on whether the density in question is for electrons, different ions, or the total plasma mass.

[34] Figures 6c and 6d show the value of n_e derived from the f_{pe} and $f_{\rm UHR}$ lines that are visible in the plasma wave spectra shown in Figure 2a. On the outbound leg, the value of n_e was 500 cm^{-3} at the inner edge of the plasmapause ($L = 3.5$), 40 cm^{-3} at the outer edge of the plasmapause ($L = 3.8$), 20 cm^{-3} at the outer edge of the plasma trough ($L = 5.7$), and

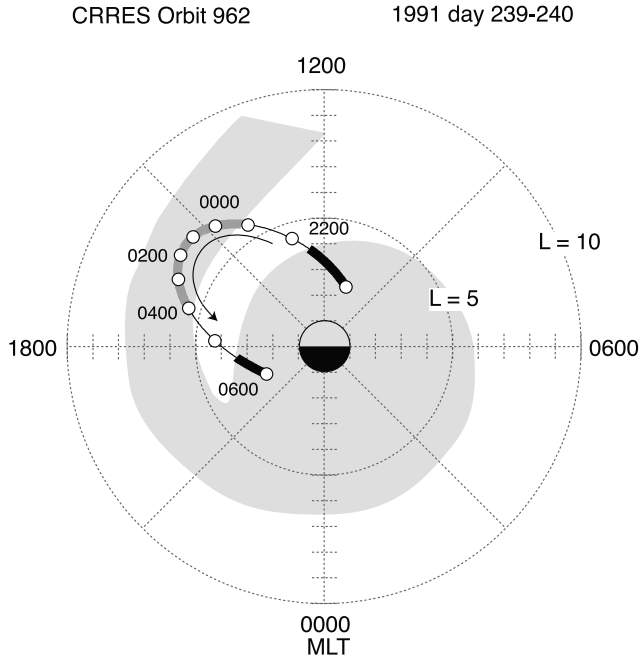

Figure 5. *L*-MLT plots of CRRES position for the time period covered in Figure 2. Different line types are used for three regions identified from the electron number density data: the plasmasphere (thick black line), the plasma trough (thin black line), and the plasma plume (thick gray line). The *L*-MLT coordinates are based on a centered dipole.

60 cm^{-3} at the inner edge of the plasma plume ($L = 5.9$). On the inbound leg, the value of n_e was 590 cm^{-3} at the inner edge of the plasmapause ($L = 3.3$), 170 cm^{-3} at the outer edge of the plasmapause ($L = 3.4$), 35 cm^{-3} at the outer edge of the plasma trough ($L = 5.0$), and 130 cm^{-3} at the inner edge of the plasma plume ($L = 5.4$). In summary, the electron density changed by a factor of 3 or 12 across the p-sphere/p-trough boundary and by a factor of 3 or 4 across the p-trough/p-plume boundary.

[35] Figures 6c and 6d also show the total mass density ρ_{total} (heavy dots) corresponding to f_{T1}. The conversion of f_{T1} to ρ_{total} was done using the technique described by *Takahashi et al.* [2004, 2006]. Briefly, we specify the background magnetic field by a numerical model and the mass distribution along a field line by an analytical function and numerically solve the MHD wave equation of *Singer et al.* [1981] to get the relationship between the mass density and the standing wave frequency. Here we used the TS05 magnetic field model [*Tsyganenko and Sitnov*, 2005] with the required solar wind parameters taken from the tabulated values provided by *Qin et al.* [2007]. The field line mass distribution adopted the result of *Takahashi et al.* [2004] and is given by

$$\rho_{total} = \rho_{eq}(LR_E/R)^{0.5} \quad (5)$$

where ρ_{eq} is the equatorial mass density and R is the geocentric distance to the field line.

[36] As expected from Figures 6a and 6b, ρ_{total} decreases monotonically with increasing L without sudden changes across the sharp gradient found for n_e. As a consequence, there is a large difference between the n_e (cm^{-3}) and ρ_{total} (amu cm^{-3}) data points in the plasma trough. By contrast, the data points overlap in the plasma plume. The only way to account for the different behaviors of ρ_{total} and n_e is to assume vastly different ion compositions in the high-n_e (plasma plume) and low-n_e (plasma trough) regions. If the ion composition had remained the same, the standing wave frequency f_{T1} would have changed by a factor of $\sim$2 across the trough/plume corresponding to the observed n_e changes, since Alfvén wave velocity is given by $B(\mu_0\rho_{total})^{-1/2}$ and B varies smoothly as L^{-3}.

[37] Figures 6e and 6f show the average ion mass M (see equation (4)) defined at the satellite position. Three horizontal lines are drawn for hypothetical single-ion plasmas: all-H^+ plasma ($M = 1.0$ amu); all-He^+ plasma ($M = 4.0$ amu), and all-O^+ plasma ($M = 16.0$ amu). The value of M is well below 4 amu (mass of He^+) in the plume whereas it is between 4 amu and 16 amu (mass of O^+) in the plasma trough. The values of M exceeding 4.0 amu in the plasma trough imply that O^+ ions contribute to the mass density in this region.

[38] Although most data points in Figures 6e and 6f lie between $M = 1$ amu and $M = 16$ amu, there are some data points that lie outside these limits as noted in our previous statistical study of CRRES data [*Takahashi et al.*, 2006]. Between the two parameters n_e and ρ_{total} that define M, the latter is more likely the cause of the unphysical values of M. There are a few possible sources of the error in M. First, the Alfvén wave frequency was determined from a short data segment, 8-min in the present study, not much longer than the period of the waves. No matter what spectral analysis technique we use, a relatively large error is inevitable in this approach. This is compounded by the fact that magnetospheric standing Alfvén waves are never stationary in phase or amplitude as a result of the temporal variation of the strength of the source mechanism. When amplitude and phase vary, the spectrum of the waves broadens and the spectral peak may occur at a frequency different from the true eigenfrequency of the local field line. Second, the accuracy of ρ_{total} depends on the accuracy of the magnetic field model and the field line mass distribution model. As we discussed previously [*Takahashi et al.*, 2006], existing magnetic field models often differ significantly from observation and, despite the significant progress we made regarding the field line mass distribution in recent years [*Denton et al.*, 2004; *Takahashi and Denton*, 2007], it is difficult to determine the distribution for individual wave events. Despite the errors, there is little question that the magnetoseismology technique gives us valuable information about heavy ions in the magnetosphere. As we described in section 1, there is significant interest in determining the number of O^+ ions within the equatorial magnetosphere in relation to various processes that regulate the location and strength of the ring current and radiation belts.

[39] Figure 7 shows additional parameters that we can derive by combining n_e and ρ_{total} (a summary of the parameters is given in Table 1). For simplicity, we assume that the plasma consists of the three ion species H^+, He^+, and O^+, which is not unrealistic according to previous observations by DE-1 and GEOS-1 and -2. Having only two known parameters, n_e and ρ_{total}, we cannot uniquely

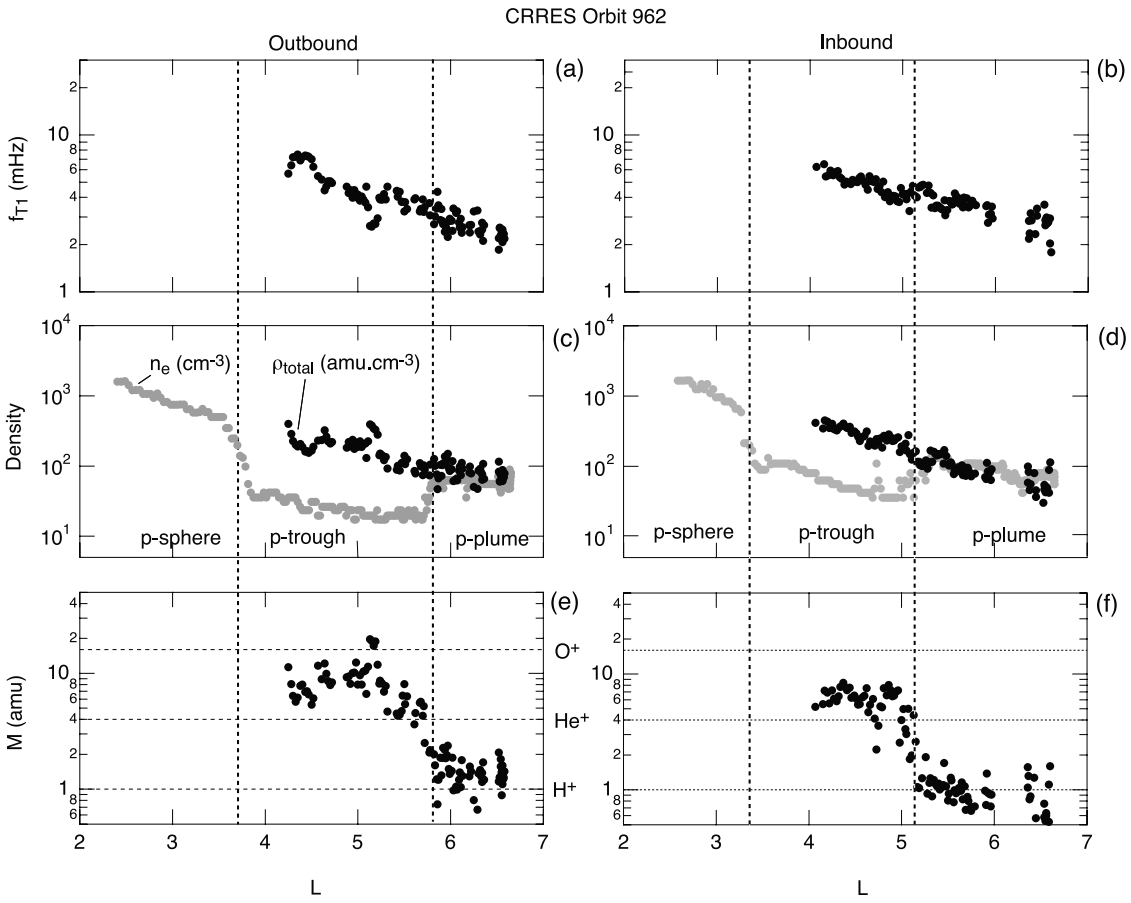

Figure 6. Parameters extracted from the plasma wave and ULF wave spectra plotted as a function of the dipole L of CRRES for the inbound and outbound legs of orbit 962. The vertical dashed lines indicate the region boundaries that are identified from the n_e data. (a, b) The fundamental toroidal frequency. (c, d) The electron number density (n_e) and the plasma mass density (ρ_{total}). (e, f) The average ion mass (M). The horizontal lines indicate the mass of singly ionized hydrogen, helium, and oxygen ions.

determine the density of the three ions. However, it is possible to place limits to the density for each ion. For O^+, its minimum possible density is obtained by assuming the H^+ density to be zero, i.e.,

$$n_{O\_min} = \frac{n_e(M - m_{He})}{m_O - m_{He}} \tag{6}$$

and its maximum possible density is obtained by assuming the He^+ density to be zero

$$n_{O\_max} = \frac{n_e(M - m_H)}{m_O - m_H} \tag{7}$$

[40] Note that the right-hand side of the equations (6) and (7) gives a negative value for $M < 4$ amu and $M < 1$ amu, respectively, in which case we set the value of the left-hand side to zero.

[41] Using the above density limits, the limits of the mass density carried by O^+ ions can be written as $\rho_{O\_min} = m_O n_{O\_min}$ and $\rho_{O\_max} = m_O n_{O\_max}$. Similarly, the limits of the fractional values can be obtained as n_{O_min}/n_e and n_{O_max}/n_e for the number density and as $\rho_{O\_min}/\rho_{total}$ and $\rho_{O\_max}/\rho_{total}$ for the mass density.

[42] Alternatively, if we opt to specify the n_{He}-to-n_e ratio ($=\eta$), then the O^+ density is given by

$$n_O(\eta) = \frac{n_e\{M - m_H - \eta(m_{He} - m_H)\}}{m_O - m_H} \tag{8}$$

[43] Given the weak dependence of the He^+ density on geomagnetic activity level [*Young et al.*, 1982], adopting a fixed value of η may be a reasonable approach.

[44] Figures 7a and 7b compare n_e and n_O. The vertical error bars connect n_{O_min} and n_{O_max} to indicate the possible range of n_O for each estimate of f_{T1}. The dots are the values given by equation (8) assuming $\eta = 0.07$ [*Anderson et al.*, 1996]. In the plasma trough n_O has small errors and decreases with L, following the trend of n_e. In the middle of the trough region, the value of n_O is $\sim$10 cm^{-3} for both legs. In the plasma plume, only the upper limit of n_O is defined for most data points, which means that the derived mass density in this region could be accounted for using only H^+ and He^+ ions. Consequently, there is a huge uncertainty in the value of n_O in the plume. However, since

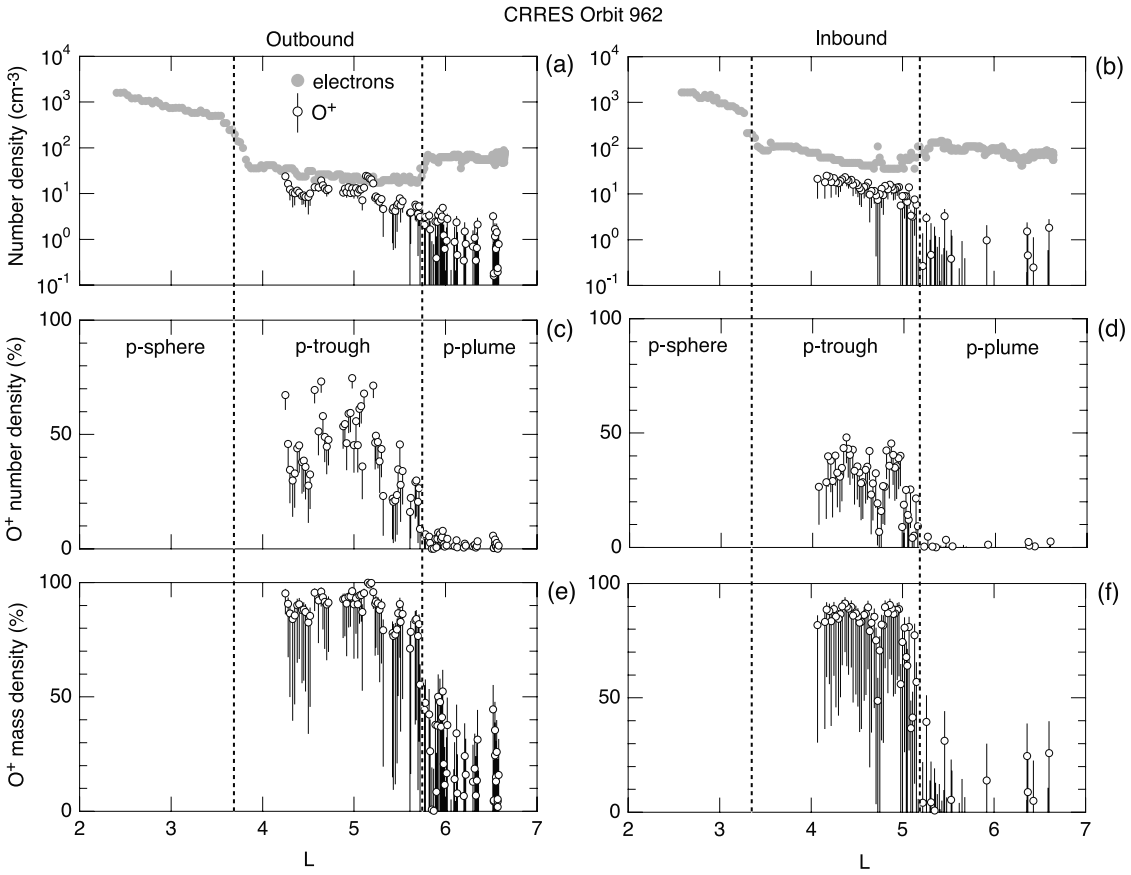

Figure 7. Plasma density parameters for the outbound and inbound legs of CRRES orbit 962 plotted as a function of dipole L. (a, b) Number density of electrons and O^+ ions. The O^+ density is shown by vertical bars, with the upper (lower) limit corresponding to a hypothetical O^+-H^+ (O^+-He^+) plasma. The white dots correspond to the assumption $n_{He}/n_e = 0.07$. (c, d) Fractional O^+ ion number density. (e, f) Fractional O^+ ion mass density.

n_{O_max} in the plume is on average a decreasing function of L, no strong source of O^+ appears to exist outward of $L \sim 5$. With the assumed value of η, $n_O(\eta)$ is close to n_{O_max} in both the plasma trough and plasma plume.

[45] Figures 7c and 7d show the n_O/n_e ratio. This parameter also shows a clear difference between the plasma trough and the plasma plume. In the trough the O^+ ions account for ~50% (outbound leg) to ~30% (inbound leg) of the ion number density. In the plume the O^+ ions account for less than 10% of the ion number density.

[46] Figures 7e and 7f show the fractional mass density carried by O^+, given by $n_O m_O/\rho_{total}$. In the plasma trough, $n_O m_O/\rho_{total}$ is mostly in the range of 50 to 100%, which means that O^+ carries most of the observed mass density. In the plasma plume, $n_O m_O/\rho_{total}$ is below 50%, which means that the lighter ions, H^+ and He^+, carry more than half of the mass density.

3. Discussion

3.1. Heavy Ions in the Inner Magnetosphere

[47] We have shown above that O^+ was the dominant ion species in the plasma trough in mass density and possibly in number density as well. Here we make a quantitative comparison of our results with previous results on heavy ions and comment on possible mechanisms for formation of the oxygen-rich region in the inner magnetosphere. The standard scenario [e.g., *Nishida*, 1966] for the formation of the plasmasphere is that plasmasphere and plasma trough flux tubes have been in the inner middle magnetosphere and closed for some time, so they are close to being in

Table 1. Magnetoseismology Analysis Results for CRRES Orbit 962[a]

Physical Quantity	Plasma Trough Inbound (Outbound)	Plasma Plume Inbound (Outbound)
M (amu)	8.1 (6.1)	1.4 (0.97)
n_{O_max} (cm^{-3})	11 (15)	1.5 (0)
n_{O_min} (cm^{-3})	7.8 (7.9)	0 (0)
n_{O_max}/n_e (%)	48 (34)	3 (0)
n_{O_min}/n_e (%)	34 (18)	0 (0)
ρ_{O_max} (amu cm^{-3})	180 (–)	23 (–)
ρ_{O_min} (amu cm^{-3})	120 (130)	0 (0)
$\rho_{O\_max}/\rho_{total}$ (%)	93 (89)	30 (–)
$\rho_{O\_min}/\rho_{total}$ (%)	67 (46)	0 (0)

[a]The median values are listed ("–" indicates undefined quantity).

equilibrium with the upper ionosphere. Plasma trough flux tubes have recently (within the past few hours) convected in from the plasma sheet, so they contain plasma sheet plasma (both hot and cold). Thus the trough and plume flux tubes, although right next to each other, have very different histories and it is no surprise that they contain very different types of plasma. However, when an ion species is preferentially transported from the ionosphere to the magnetosphere or accelerated in a limited region in space and in a time-dependent manner, the spatial distribution of the ion species may become more complex than what the standard scenario predicts.

[48] The DE-1 spacecraft (a polar orbiting spacecraft with an apogee of 4.6 R_E) measured the flux of low-energy (<50 eV) ions with the Retarding Ion Mass Spectrometer (RIMS) instrument [*Chappell et al.*, 1981]. The RIMS instrument was not suited for measuring ions in the low-density region (i.e., the plasma trough) because of floating spacecraft potentials. A major finding with RIMS was the formation of an oxygen torus at the outer edge of the plasmapause during geomagnetically active periods. *Horwitz et al.* [1984] reported the spatial and temporal development of the torus for representative orbits. *Roberts et al.* [1987] conducted a statistical analysis of the torus and found that the oxygen number density tends to peak between $L = 2$ and $L = 5$.

[49] A scenario for the torus formation that is favored by *Roberts et al.* [1987] is as follows. The outer plasmasphere interacts with the more energetic ring current particles either through Coulomb collision or through wave-particle interactions [*Horwitz et al.*, 1986]. This interaction will heat the ionospheric plasma and raise the scale height of ionospheric ions, which leads to an elevated O^+/H^+ ratio in the equatorial magnetosphere. This scenario explains the elevated O^+ population adjacent to the (electron and H^+) plasmapause. However, is it is not clear if the process explains the elevated O^+ density ~2 R_E away from the plasmapause up to the inner edge of the plasma plume (see Figures 7a and 7b). Therefore the elevation of the O^+/H^+ ratio throughout the electron trough region may be better explained if there is a significant contribution of O^+ ions from the ring current (with keV energy) rather than all the O^+ being plasmaspheric (eV energy).

[50] The GEOS-1 (1.3 × 7.0 R_E elliptical orbit with 26° inclination) and GEOS-2 (geostationary) spacecraft each carried an ion composition experiment (ICE) to measure the flux of thermal energy (0.9−15.9 keV/e) ions. *Balsiger et al.* [1980] examined the GEOS/ICE data acquired during geomagnetic storms and found that the O^+ number density becomes large, often comparable to the H^+ density, both during the main and recovery phases of a storm. During a storm with a *Dst* minimum of −226 nT that occurred in August 1978, the O^+ number density became as high as ~10 cm^{-3}, which is comparable to our estimates in the plasma trough region.

[51] *Young et al.* [1982] reported a comprehensive statistical study of ion composition for $6 < L < 7$ based on the GEOS/ICE data. They noted that the quiet-time ($Kp < 2_o$) ion composition changed dramatically from solar minimum (May 1977) values of 93% H^+, 5% O^+, and 1% He^+ to solar maximum (November 1979) values of 48% H^+, 44% O^+, and 5% He^+. Between the two epochs the total ion density and mean ion mass increased from 0.29 cm^{-3} to 0.63 cm^{-3} and from 1.9 amu to 8.2 amu, respectively. These changes correspond to a mass density increase of approximately from 0.55 amu cm^{-3} to 5.2 amu cm^{-3}, that is, a change by a factor of 9. Young et al. attributed the long-term changes to a strong dependence of the O^+ density on solar EUV flux (represented by $F_{10.7}$, which is given in units of 10^{-22} $Wm^{-2}Hz^{-1}$). Young et al. also found a positive correlation between O^+ density and *Kp* (and *Ap*) (a similar correlation was found for other ions as well) and obtained the following empirical formula:

$$n_O = 0.011 \exp[0.24Kp + 0.011F_{10.7}] \pm 0.16\,\mathrm{cm}^{-3} \quad (9)$$

$$n_O/n_H = 4.5 \times 10^{-2} \exp[0.17Kp + 0.010F_{10.7}] \pm 0.21 \quad (10)$$

[52] By substitution of $Kp = 2-6$ and $F_{10.7} = 200$ for our storm event (see Figures 1 and 4), we obtain $n_O = 0.16 - 0.42$ cm^{-3} and $n_O/n_H = 0.48 - 0.92$. The n_O range is lower than our estimate ~10 cm^{-3} (see Table 1) for the trough region. However, this could simply be a result of an inward density gradient: our trough region was $L = 4-6$ while the GEOS results were for $L = 6-7$. On the other hand, our density ratio n_O/n_H (0.46−0.93) is in good agreement with equation (10). It appears that both high geomagnetic activity and the high solar EUV flux contributed to the high O^+ density observed by CRRES on orbit 962.

[53] Our observation differs from the GEOS observation in that we have n_e data to identify the plasma regions. In our study the average ion mass differed significantly between the plasma plume and the plasma trough, meaning that heavy ions had a different spatial distribution than light ions. This is possible if the energy differs between them. The drainage plume represents a cold plasma population that consists of H^+-dominant ionospheric plasma that was energized. This plasma is transported primarily by the $\mathbf{E} \times \mathbf{B}$ drift. On the other hand, heavy ions in the plasma trough must have substantially higher energy so that their motion is governed by the magnetic field gradient and curvature drift in addition to the $\mathbf{E}\times\mathbf{B}$ drift [*Takahashi and Iyemori*, 1989]. It is possible that the O^+ ions gained energy in the plasma sheet and drifted into the inner magnetosphere as described by *Nosé et al.* [2005].

3.2. Detection of the Plasmapause and Plasma Plume Using Magnetoseismology

[54] Recent ground-based magnetoseismology studies addressed the mass density structure and the ion composition in the inner magnetosphere. For example, *Dent et al.* [2006] combined mass density obtained from the ground-based ULF cross-phase technique and electron number density determined from the RPI instrument on the IMAGE spacecraft to derive the mean ion mass in the inner magnetosphere ($L < 7$). During a moderate storm ($Dst > -80$ nT) in May 2001 (near a solar maximum), the average ion mass in the $L = 4.0-5.0$ region was estimated to be between ~1.8 and 4.1 amu. Dent et al. attributed this observation to the ion torus reported from the DE-1 RIMS studies referenced above. Note that their estimate has some uncertainties

arising from different locations for mass density (ground) and electron density (spacecraft) measurements along with assumptions for the background magnetic field to relate the observed field line resonance frequencies to mass densities.

[55] *Fraser et al.* [2005] revisited one of DE-1's passes through an oxygen torus reported by *Horwitz et al.* [1984] and showed that O^+ ions contributed significantly to the mass density just outside the H^+ plasmapause so that the plasmapause identified from ρ_{total} was located almost two L shells outward of the H^+ plasmapause. Fraser et al. also modeled the frequency of standing Alfvén waves based on the derived total mass density and indicated that the frequency did not exhibit a sudden change across the H^+ plasmapause (*Fraser et al.* [2005] did not compare the density data with ULF wave observations). Since H^+ is usually the dominant ion species in terms of number density, n_H (or n_e as its proxy) is often used to define the plasmapause [*Carpenter*, 1966; *Chappell et al.*, 1970; *Carpenter and Anderson*, 1992; *Moldwin et al.*, 2002]. The work by Fraser et al. thus cautions against the use of the term plasmapause without specifying whether the quantity in question is n_e or ρ_{total}. Recent studies combining n_e measurements with various experiments and mass density estimates using the ground-based magnetoseismology technique [*Menk et al.*, 2004; *Dent et al.*, 2006; *Grew et al.*, 2007] confirmed that n_e and ρ_{total} often exhibit a large difference outside the n_e plasmapause during geomagnetically active periods. Although we did not determine the mass density near the plasmapause, our estimates of ρ_{total} are in strong support of the argument by Fraser et al. that the heavy ion density needs to be considered in discussing standing Alfvén waves in the inner magnetosphere.

[56] CRRES crossed the boundary between the plasma trough and what we believe to be a drainage plume. We found no rapid change in f_{T1}, which implied that the mass density did not change rapidly across the plasma trough and plasma plume boundary. This means that H^+ is the dominant ion species in the plasma plume similar to the plasmasphere. This is not surprising since the plume is an extension of the plasmasphere that is formed by the temporal variation of the magnetospheric electric field upon co-rotating plasmaspheric cold plasma.

[57] We now address the effectiveness of the magnetoseismology technique in detecting a plasma plume. Recently, *Abe et al.* [2006] reported an attempt to use ground ULF pulsations to detect the signature of a plasma plume that was visible in the He^+ images of the magnetosphere taken by the IMAGE spacecraft [*Sandel et al.*, 2000]. The primary parameter in their study was the ratio of pulsation power between the two stations CHD (L = 5.55) and TIK (L = 5.98), given as a function of frequency. The frequency dependence of the ratio differed between two selected time intervals. On the basis of the model of *Baransky et al.* [1985], *Abe et al.* [2006] interpreted one interval as corresponding to entry of the ground stations into the plume region through the earthward edge of the plume (anti-earthward density gradient) and the other as corresponding to exit from the plume through the anti-earthward edge of the plume (earthward density gradient, such as the plasmapause). An L-profile of the field-line resonance frequency, which would have been verification of the plume detection, was not available for the intervals reported.

[58] Our CRRES observations on orbit 962 indicate that it would have been impossible to detect the signature of the plume encountered on this orbit on the ground since CRRES observed no sudden change in f_{T1} across the plume boundary. Our definition of the plume was based on electron number density, so we cannot directly compare our results with that of *Abe et al.* [2006], who relied on He^+ density to identify a plume. However, based on the DE-1 RIMS studies reporting that the n_{He}/n_H ratio is less variable than the n_O/n_H ratio [*Horwitz et al.*, 1984; *Roberts et al.*, 1987; *Craven et al.*, 1997], we believe that He^+ had a plume structure quite similar to the H^+ plume.

[59] One caution, however, in generalizing our results to the case of all plumes, is that the study of *Takahashi et al.* [2006] showed a large variation in the average ion mass M in the plasmatrough with variation across the entire range 1−16 amu. The average value of M in the plasmatrough was about 3.5 amu (from Figure 8 of their paper), and this is less than the values of 6−8 amu we inferred for CRRES orbit 962 (Table 1). If M has a lower value in the plasmatrough, there will be a closer relation between boundaries based on observations of n_e and those based on observations of ρ_{total}. For high geomagnetic activity, which is favorable for the formation of plumes, the average value of M is higher [Figure 11 of *Takahashi et al.*, 2006], yet there still is a large variation in M even for high geomagnetic activity. Therefore we cannot rule out the possibility that plumes could be identified by magnetoseismology in some cases. However, we have certainly shown that it is more difficult to identify a plume using observations of ρ_{total} than using observations of n_e.

4. Conclusions

[60] In conclusion, we have applied a magnetoseismology technique to investigate the ion composition for CRRES orbit 962 (27−28 August 1991), which occurred during a geomagnetic storm and included passes through the three regions identified in terms of electron density n_e: outer plasmasphere, the plasma trough, and a plasma plume. In the magnetoseismology analysis we determined the fundamental frequency of the toroidal standing Alfvén waves (f_{T1}) from the electric and magnetic field data and then inferred the corresponding total mass density ρ_{total} at the satellite by solving an MHD wave equation with a realistic magnetic field model and realistic assumption on mass distribution along the field line. From n_e and ρ_{total}, we derived other parameters assuming that the plasma consisted of three ions, H^+, He^+, and O^+. We found that H^+ is dominant in the plasma plume while O^+ is dominant in the plasma trough. In the plasma trough (L = 3.5−5.5) O^+ ions are found to have a number density of ~10 cm^{-3}, and to account for ~50% of the number density and ~90% of the mass density. As a result of the dominance of the O^+ ions in the plasma trough, the mass density varied little as the spacecraft traversed the plume-trough boundary. Our study confirmed the presence of a plasma trough with high oxygen concentration during a geomagnetic active period. In addition, we showed that the particular plasma plume was a structure relevant to light ions (H^+ and probably He^+) but not to heavy ions or to total mass density. Consequently, the plume inner edge that was encountered by CRRES

would not have been recognized as a plasma boundary in ULF wave signals detected on the ground.

[61] **Acknowledgments.** This work was supported by NSF grant ATM-0632740. Work at JHU/APL was also supported by NSF grant ATM-0318173. Work at Dartmouth was also supported by NSF grants ATM-0503371. R.E.D. and W.J.H. also received support from the Center for Integrated Space Weather Modeling (CISM), an NSF Science and Technology Center funded via ATM-0120950.

[62] Amitava Bhattacharjee thanks Martin Wuest and Mike Schulz for their assistance in evaluating this paper.

References

Abe, S., H. Kawano, J. Goldstein, S. Ohtani, S. I. Solovyev, D. G. Baishev, and K. Yumoto (2006), Simultaneous identification of a plasmaspheric plume by a ground magnetometer pair and IMAGE extreme ultraviolet imager, *J. Geophys. Res.*, *111*, A11202, doi:10.1029/2006JA011653.

Anderson, R. R., D. A. Gurnett, and D. L. Odem (1992), The CRRES plasma wave experiment, *Spacecr. Rockets*, *29*(4), 570–574.

Anderson, B. J., R. E. Denton, G. Ho, D. C. Hamilton, S. A. Fuselier, and R. J. Strangeway (1996), Observational test of local proton cyclotron instability in the Earth's magnetosphere, *J. Geophys. Res.*, *101*(A10), 21,527–21,543.

Balsiger, H., P. Eberhardt, J. Geiss, and D. T. Young (1980), Magnetic storm injection of 0.9- to 16-keV/e solar wind terrestrial ions into the high-altitude magnetosphere, *J. Geophys. Res.*, *85*(A4), 1645–1662.

Baransky, L. N., Y. E. Borovkov, M. B. Gokhberg, S. M. Krylov, and V. A. Troitskaya (1985), High resolution method of direct measurement of the magnetic field lines' eigenfrequencies, *Planet. Space Sci.*, *33*(12), 1369–1374.

Bendat, J. S., and A. G. Piersol (1971), *Random Data: Analysis and Measurement Procedures*, 407 pp., John Wiley, New York.

Bräysy, T., K. Mursula, and G. Marklund (1998), Ion cyclotron waves during a great magnetic storm observed by Freja double-probe electric field instrument, *J. Geophys. Res.*, *103*(A3), 4145–4155.

Carpenter, D. L. (1966), Whistler study of the plasmapause in the magnetosphere: 1. Temporal variations in the position of the knee and some evidence on plasma motions near the knee, *J. Geophys. Res.*, *71*(3), 693–709.

Carpenter, D. L., and R. R. Anderson (1992), An ISEE/whistler model of equatorial electron density in the magnetosphere, *J. Geophys. Res.*, *97*(A2), 1097–1108.

Chappell, C. R. (1974), Detached plasma regions in the magnetosphere, *J. Geophys. Res.*, *79*(13), 1861–1870.

Chappell, C. R., K. K. Harris, and G. W. Sharp (1970), A study of the influence of magnetic activity on the location of the plasmapause as measured by OGO 5, *J. Geophys. Res.*, *75*(1), 50–56.

Chappell, C. R., S. A. Fields, C. R. Bauer, J. H. Hoffman, W. B. Hanson, W. W. Wright, H. D. Hammack, G. R. Carignan, and A. F. Nagy (1981), The retarding ion mass spectrometer on Dynamics Exploler-A, *Space Sci. Instrum.*, *5*, 477.

Chi, P. J., and C. T. Russell (2005), Travel-time magnetoseismology: Magnetospheric sounding by timing the tremor in space, *Geophys. Res. Lett.*, *32*, L18108, doi:10.1029/2005GL023441.

Craven, P. D., D. L. Gallagher, and R. H. Comfort (1997), Relative concentration of He^+ in the inner magnetosphere as observed by the DE 1 retarding ion mass spectrometer, *J. Geophys. Res.*, *102*(A2), 2279–2289.

Cummings, W. D., R. J. O'Sullivan, and P. J. Coleman Jr. (1969), Standing Alfvén waves in the magnetosphere, *J. Geophys. Res.*, *74*(3), 778–793.

Daglis, I. A., R. M. Thorne, W. Baumjohann, and S. Orsini (1999), The terrestrial ring current: Origin, formation, and decay, *Rev. Geophys.*, *37*(4), 407–438.

Dent, Z. C., I. R. Mann, J. Goldstein, F. M. Menk, and L. G. Ozeke (2006), Plasmaspheric depletion, refilling, and plasmapause dynamics: A coordinated ground-based and IMAGE satellite study, *J. Geophys. Res.*, *111*, A03205, doi:10.1029/2005JA011046.

Denton, R. E., and D. L. Gallagher (2000), Determining the mass density along magnetic field lines from toroidal eigenfrequencies, *J. Geophys. Res.*, *105*(A12), 27,717–27,725.

Denton, R. E., M. R. Lessard, R. Anderson, E. G. Miftakhova, and J. W. Hughes (2001), Determining the mass density along magnetic field lines from toroidal eigenfrequencies: Polynomial expansion applied to CRRES data, *J. Geophys. Res.*, *106*(A12), 29,915–29,924.

Denton, R. E., K. Takahashi, R. R. Anderson, and M. P. Wuest (2004), Magnetospheric toroidal Alfvén wave harmonics and the field line distribution of mass density, *J. Geophys. Res.*, *109*, A06202, doi:10.1029/2003JA010201.

Elkington, S. R., M. K. Hudson, and A. A. Chan (1999), Acceleration of relativistic electrons via drift-resonant interaction with toroidal-mode Pc-5 ULF oscillations, *Geophys. Res. Lett.*, *26*(21), 3273–3276.

Elphic, R. C., L. A. Weiss, M. F. Thomsen, D. J. McComas, and M. B. Moldwin (1996), Evolution of plasmaspheric ions at geosynchronous orbit during times of high geomagnetic activity, *Geophys. Res. Lett.*, *23*(16), 2189–2192.

Erlandson, R. E., and A. J. Ukhorskiy (2001), Observations of electromagnetic ion cyclotron waves during geomagnetic storms: Wave occurrence and pitch angle scattering, *J. Geophys. Res.*, *106*(A3), 3883–3896, doi:10.1029/2000JA000083.

Fraser, B. J., J. L. Horwitz, J. A. Slavin, Z. C. Dent, and I. R. Mann (2005), Heavy ion mass loading of the geomagnetic field near the plasmapause and ULF wave implications, *Geophys. Res. Lett.*, *32*, L04102, doi:10.1029/2004GL021315.

Goldstein, J., and B. R. Sandel (2005), The global pattern of evolution of plasmaspheric drainage plumes, in *Global Physics of the Coupled Inner Magnetosphere*, edited by M. Schulz, H. Spence, and J. L. Burch, pp. 1–22, AGU, Washington, D. C.

Grebowsky, J. M. (1970), Model study of plasmapause motion, *J. Geophys. Res.*, *75*(22), 4329–4333.

Grew, R. S., F. W. Menk, M. A. Clilverd, and B. R. Sandel (2007), Mass and electron densities in the inner magnetosphere during a prolonged disturbed interval, *Geophys. Res. Lett.*, *34*, L02108, doi:10.1029/2006GL028254.

Horwitz, J. L., R. H. Comfort, and C. R. Chappell (1984), Thermal ion measurements of the formation of the new outer plasmasphere and double plasmapause during storm recovery phase, *Geophys. Res. Lett.*, *11*(8), 701–704.

Horwitz, J. L., L. H. Brace, R. H. Comfort, and C. R. Chappell (1986), Dual-spacecraft measurements of plasmasphere-ionosphere coupling, *J. Geophys. Res.*, *91*(A10), 11,203–11,216.

Jordanova, V. K., M. Spasojevic, and M. F. Thomsen (2007), Modeling the electromagnetic ion cyclotron wave-induced formation of detached subauroral proton arcs, *J. Geophys. Res.*, *112*, A08209, doi:10.1029/2006JA012215.

Junginger, H., G. Geiger, G. Haerendel, F. Melzner, E. Amata, and B. Higel (1984), A statistical study of dayside magnetospheric electric field fluctuations with periods between 150 and 600 s, *J. Geophys. Res.*, *89*(A7), 5495–5505.

Kale, Z. C., I. R. Mann, C. L. Waters, J. Goldstein, F. W. Menk, and L. G. Ozeke (2007), Ground magnetometer observation of a cross-phase reversal at a steep plasmapause, *J. Geophys. Res.*, *112*, A10222, doi:10.1029/2007JA012367.

Kozyra, J. U., A. F. Cravens, A. F. Nagy, E. G. Fntheim, and R. S. B. Ong (1984), Effects of energetic heavy ions on electromagnetic ion cyclotron wave generation in the plasmapause region, *J. Geophys. Res.*, *89*(A4), 2217–2233.

LeDocq, M. J., D. A. Gurnett, and R. R. Anderson (1994), Electron number density fluctuations near the plasmapause observed by the CRRES spacecraft, *J. Geophys. Res.*, *99*(A12), 23,661–23,671.

Menk, F. W., I. R. Mann, A. J. Smith, C. L. Waters, M. A. Clilverd, and D. K. Milling (2004), Monitoring the plasmapause using geomagnetic field line resonances, *J. Geophys. Res.*, *109*, A04216, doi:10.1029/2003JA010097.

Meredith, N. P., R. M. Thorne, R. B. Horne, D. Summers, B. J. Fraser, and R. R. Anderson (2003), Statistical analysis of relativistic electron energies for cyclotron resonance with EMIC waves observed on CRRES, *J. Geophys. Res.*, *108*(A6), 1250, doi:10.1029/2002JA009700.

Milling, D. K., I. R. Mann, and F. W. Menk (2001), Diagnosing the plasmapause with a network of closely spaced ground-based magnetometers, *Geophys. Res. Lett.*, *28*(1), 115–118.

Moldwin, M. B., L. Downward, H. K. Rassoul, R. Amin, and R. R. Anderson (2002), A new model of the location of the plasmapause: CRRES results, *J. Geophys. Res.*, *107*(A11), 1339, doi:10.1029/2001JA009211.

Moldwin, M. B., J. Howard, J. Sanny, J. D. Bocchicchio, H. K. Rassoul, and R. R. Anderson (2004), Plasmaspheric plumes: CRRES observations of enhanced density beyond the plasmapause, *J. Geophys. Res.*, *109*, A05202, doi:10.1029/2003JA010320.

Nishida, A. (1966), Formation of plasmapause, or magnetospheric plasma knee, by the combined action of magnetospheric convection and plasma escape from the tail, *J. Geophys. Res.*, *71*(23), 5669–5679.

Nosé, M., S. Ohtani, K. Takahashi, A. T. Y. Lui, R. W. McEntire, D. J. Williams, S. P. Christon, and K. Yumoto (2001), Ion composition of the near-Earth plasma sheet in storm and quiet intervals: Geotail/EPIC measurements, *J. Geophys. Res.*, *106*(A5), 8391–8404.

Nosé, M., K. Takahashi, S. Ohtani, S. P. Christon, and R. W. McEntire (2005), Dynamics of ions of ionospheric origin during magnetic storms: Their acceleration mechanism and transport path to ring current, in *The*

Inner Magnetosphere: Physics and Modeling, *Geophysical Monograph Ser.*, vol. 155, edited by T. I. Pulkkinen, N. A. Tsyganenko, and R. H. W. Friedel, pp. 61–71, AGU, Washington, D. C.

Obayashi, T., and J. A. Jacobs (1958), Geomagnetic pulsations and the earth's outer atmosphere, *Geophys. J. R. Astron. Soc.*, *1*, 53–63.

Press, W. H., B. P. Flannery, S. A. Teukolsky, and W. T. Vetterling (1986), *Numerical Recipes*, Cambridge Univ. Press, New York.

Qin, Z., R. E. Denton, N. A. Tsyganenko, and S. Wolf (2007), Solar wind parameters for magnetospheric magnetic field modeling, *Space Weather*, *5*, S11003, doi:10.1029/2006SW000296.

Radoski, H. R., and R. L. Carovillano (1966), Axisymmetric plasmasphere resonances: Toroidal mode, *Phys. Fluids.*, *9*(2), 285–291.

Roberts, W. T., Jr., J. L. Horwitz, R. H. Comfort, C. R. Chappell, J. H. Waite Jr., and J. L. Green (1987), Heavy ion density enhancements in the outer plasmasphere, *J. Geophys. Res.*, *92*(A12), 13,499–13,512.

Sandel, B. R., et al. (2000), The extreme ultraviolet imager investigation for the IMAGE mission, *Space Sci. Rev.*, *91*(1–2), 197–242, doi:10.1023/A:1005263510820.

Sandel, B. R., R. A. King, W. T. Forrester, D. L. Gallagher, A. L. Broadfoot, and C. C. Curtis (2001), Initial results from the IMAGE extreme ultraviolet imager, *Geophys. Res. Lett.*, *28*(8), 1439–1442.

Singer, H. J., D. J. Southwood, R. J. Walker, and M. G. Kivelson (1981), Alfvén wave resonances in realistic magnetospheric magnetic field geometry, *J. Geophys. Res.*, *86*(A6), 4589–4596.

Singer, H. J., W. P. Sullivan, P. Anderson, F. Mozer, P. Harvey, J. Wygant, and W. McNeil (1992), Fluxgate magnetometer instrument on the CRRES, *J. Spacecraft*, *29*(4), 599–601.

Spasojevic, M., J. Goldstein, D. L. Carpenter, U. S. Inan, B. R. Sandel, M. B. Moldwin, and B. W. Reinisch (2003), Global response of the plasmasphere to a geomagnetic disturbance, *J. Geophys. Res.*, *108*(A9), 1340, doi:10.1029/2003JA009987.

Takahashi, K., and R. E. Denton (2007), Magnetospheric seismology using multiharmonic toroidal waves observed at geosynchronous orbit, *J. Geophys. Res.*, *112*, A05204, doi:10.1029/2006JA011709.

Takahashi, S., and T. Iyemori (1989), Three-dimensional tracing of charged particle trajectories in a realistic magnetospheric model, *J. Geophys. Res.*, *94*(A5), 5505–5509.

Takahashi, K., R. E. Denton, and D. Gallagher (2002), Toroidal wave frequency at $L = 6–10$: AMPTE/CCE observations and comparison with theoretical model, *J. Geophys. Res.*, *107*(A2), 1020, doi:10.1029/2001JA000197.

Takahashi, K., R. E. Denton, R. R. Anderson, and W. J. Hughes (2004), Frequencies of standing Alfvén wave harmonics and their implication for plasma mass distribution along geomagnetic field lines: Statistical analysis of CRRES data, *J. Geophys. Res.*, *109*, A08202, doi:10.1029/2003JA010345.

Takahashi, K., R. E. Denton, R. R. Anderson, and W. J. Hughes (2006), Mass density inferred from toroidal wave frequencies and its comparison to electron density, *J. Geophys. Res.*, *111*, A01201, doi:10.1029/2005JA011286.

Tsyganenko, N. A., and M. I. Sitnov (2005), Modeling the dynamics of the inner magnetosphere during strong geomagnetic storms, *J. Geophys. Res.*, *110*, A03208, doi:10.1029/2004JA010798.

Ukhorskiy, A. Y., B. J. Anderson, P. C. Brandt, and N. A. Tsyganenko (2006), Storm time evolution of the outer radiation belt: Transport and losses, *J. Geophys. Res.*, *111*, A11S03, doi:10.1029/2006JA011690.

Waters, C. L., F. W. Menk, and B. J. Fraser (1991), The resonance structure of low latitude Pc3 geomagnetic pulsations, *Geophys. Res. Lett.*, *18*(12), 2293–2296.

Wygant, J. R., P. R. Harvey, D. Pankow, F. S. Mozer, N. Maynard, H. Singer, M. Smiddy, W. Sullivan, and P. Anderson (1992), CRRES electric field/Langmuir probe instrument, *J. Spacecraft*, *29*(4), 601–604.

Young, D. T., H. Balsiger, and J. Geiss (1982), Correlation of magnetospheric ion composition with geomagnetic and solar activity, *J. Geophys. Res.*, *87*(A11), 9077–9096.

R. R. Anderson, Department of Physics and Astronomy, University of Iowa, Room 653, Iowa City, IA 52242-1479, USA. (roger-r-anderson@uiowa.edu)

R. E. Denton, Department of Physics and Astronomy, Dartmouth College, 6127 Wilder Laboratory, Hanover, NH 03755-3528, USA. (richard.e.denton@dartmouth.edu)

W. J. Hughes, Department of Astronomy, Boston University, 725 Commonwealth Avenue, Boston, MA 02215-0000, USA. (hughes@bu.edu)

S. Ohtani and K. Takahashi, Applied Physics Laboratory, Johns Hopkins University, 11100 Johns Hopkins Road, MS MP3-E128, Laurel, MD 20723-6099, USA. (kazue.takahashi@jhuapl.edu)